White Rose Research Online

eprints@whiterose.ac.uk
https://eprints.whiterose.ac.uk
Universities of Leeds, Sheffield and York

Deposited via The University of York.

White Rose Research Online URL for this paper:
https://eprints.whiterose.ac.uk/id/eprint/246339/

Version: Published Version

Article:
Jernigan, Christopher M., Novak, Gordon A., Wang, Siyuan et al. (2026) Constraints on the Loss of Hydroperoxymethyl Thioformate (HPMTF) to Marine Clouds Using Aircraft Observations. ACS ES&T Air. ISSN: 2837-1402

https://doi.org/10.1021/acsestair.6c00199

Reuse
This article is distributed under the terms of the Creative Commons Attribution-NonCommercial-NoDerivs (CC BY-NC-ND) licence. This licence only allows you to download this work and share it with others as long as you credit the authors, but you can't change the article in any way or use it commercially. More information and the full terms of the licence here: https://creativecommons.org/licenses/

Takedown
If you consider content in White Rose Research Online to be in breach of UK law, please notify us by emailing eprints@whiterose.ac.uk including the URL of the record and the reason for the withdrawal request.

UNIVERSITY OF LEEDS
University of Sheffield
UNIVERSITY of York

ACS ES&T Air

Open Access
This article is licensed under CC-BY-NC-ND 4.0
pubs.acs.org/estair

Article

Constraints on the Loss of Hydroperoxymethyl Thioformate (HPMTF) to Marine Clouds Using Aircraft Observations

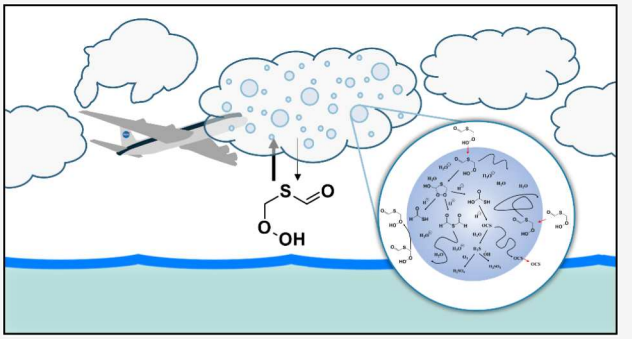
Christopher M. Jernigan,* Gordon A. Novak, Siyuan Wang, Michael A. Robinson, Adam Ahern, Osinachi Ajoku, Katherine Ball, Timothy H. Bertram, Kelvin H. Bates, Birger Bohn, Charles A. Brock, Wyndom S. Chace, Matthew Coggon, Maximilian Dollner, Michelle Färber, Zachary Finewax, Hendrik Fuchs, Georgios I. Gkatzelis, Han Huynh, Jan Kazil, Ming Lyu, Anna Novelli, Jeff Peischl, Andrew Rollins, Nell B. Schafer, Aaron Stainsby, Chelsea E. Stockwell, Patrick R. Veres, Carsten Warneke, Eleanor Waxman, Bernadett Weinzierl, Kevin Wokosin, Lu Xu, Kristen Zuraski, and Steven S. Brown

Cite This: https://doi.org/10.1021/acsestair.6c00199

Read Online

ACCESS | Metrics & More | Article Recommendations | Supporting Information

ABSTRACT: The photochemical oxidation of dimethyl sulfide (DMS) by the hydroxyl radical (OH) contributes to the production and growth of particles and cloud condensation nuclei in the marine boundary layer (MBL). DMS oxidized by OH can go on to form a stable intermediate, hydroperoxymethyl thioformate (HPMTF), which is both globally ubiquitous and efficiently lost to multiphase processes in the marine atmosphere. Recent work has shown that clouds act as a significant and irreversible loss path for HPMTF, sequestering sulfur and greatly reducing the production of long-lived, climate-relevant species (e.g., SO_2 and OCS). Until recently, there have been few observational constraints on the role of clouds in the spatiotemporal distribution of HPMTF and other soluble molecules in the MBL. Using a steady-state approximation, we determine a reactive uptake and first-order aqueous loss rate constant of HPMTF to cloud droplets of 1.2 (0.9−1.9) × 10^{-2} and 1.4 (0.4−2.2) × 10^{-1} s^{-1}, respectively. The results suggest that hydrolysis and ozonolysis are significant within cloud droplets, and their competition likely impacts the distribution of sulfate and organic acids in the marine environment.



KEYWORDS: *dimethyl sulfide, aqueous processing, marine, airborne observations, hydroperoxymethyl thioformate, sulfate, carbonyl sulfide, cloud processing*

1. INTRODUCTION

Sulfur is an essential component of Earth's biogeochemical system, with particular importance to the global climate. Depending on the source, sulfur can enter the atmosphere in a variety of reduced and oxidized forms, with a well-studied species being sulfur dioxide (SO_2). SO_2 can be emitted to the atmosphere through anthropogenic (e.g., coal combustion) or natural (e.g., passive and eruptive volcanic emissions) processes, and it can be produced through the oxidation of reduced sulfur compounds. The major natural source of reduced sulfur to the atmosphere is the ocean, with origins primarily driven by biological activity. The dominant sulfur molecule emitted from oceans is dimethyl sulfide (DMS), with an estimated emission of 22 TgS yr^{-1}.[1] The oxidation mechanism of DMS and resulting abundance and volatility of the oxidation products determine the formation and growth rates of aerosol particles to cloud condensation nuclei (CCN) in marine environments, with subsequent effects on Earth's radiative budget.[1,2] In addition, the oxidation of other marine sulfur species leads to the production of carbonyl sulfide (OCS). Accurate estimates of direct marine emissions and secondary production of OCS are critical for both modeling stratospheric aerosol concentrations, as OCS is an important precursor to stratospheric sulfate aerosol particles, and for estimating gross primary production, as OCS is readily consumed by terrestrial vegetation.[3] A large source of this uncertainty arises in the marine environment, stemming in part

Received: May 18, 2026
Revised: September 14, 2026
Accepted: September 15, 2026

Downloaded from pubs.acs.org/aeacd5/article-pdf/doi/10.1021/acsestair.6c00199/6868370/acsestair.6c00199.pdf by UNIV OF YORK user on 06 October 2026

ACS Publications

© XXXX The Authors. Published by American Chemical Society

from an incomplete understanding of the oxidation of marine sulfur gases.

Recent literature has shown that a significant fraction (>30%) of the OH-initiated oxidation of DMS over the marine atmosphere leads to the formation of a recently identified stable intermediate, hydroperoxymethyl thioformate (HPMTF, $HOOCH_2SCHO$) (Figure 1).[4−8] Since HPMTF's initial

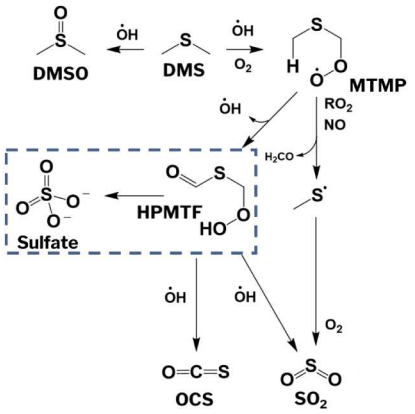


Figure 1. Simplified chemical mechanism for the gas-phase OH oxidation of dimethyl sulfide (DMS) and hydroperoxymethyl thioformate (HPMTF). Reaction products include methyl thiomethyl peroxy radical (MTMP), dimethyl sulfoxide (DMSO), sulfur dioxide (SO_2), carbonyl sulfide (OCS), and sulfate (SO_4^{2-}). The segmented box highlights simplified aqueous HPMTF reactions forming sulfate.

observation, multiple modeling, field, and laboratory investigations have been performed to understand its OH oxidation, heterogeneous uptake, and photolytic loss processes.[4,9−14] Under clear-sky conditions, HPMTF is primarily oxidized by OH with a rate constant ($k_{HPMTF + OH}$) of 1.4×10^{-11} cm^3 $molec^{-1}s^{-1}$ at 298 K to form primarily carbonyl sulfide (OCS)[10] and SO_2.[5] The OH oxidation mechanism proceeds through a variety of soluble intermediates, potentially decreasing the production of SO_2 and OCS in the marine atmosphere.[10] The heterogeneous uptake coefficient (γ) for HPMTF depends on aerosol chemical composition and has a value of 1.6×10^{-3} for deliquesced NaCl, a representative marine aerosol composition.[11] Further, HPMTF has been shown to be efficiently lost to marine clouds and the ocean surface.[4,5,12,15,16] Once reacted with an aqueous surface (e.g., cloud droplet, ocean, wetted aerosol), the condensed-phase chemistry of HPMTF is irreversible, arresting the formation of SO_2 and OCS, which are efficiently produced in the gas-phase OH oxidation of HPMTF (Figure 1).[4,10,16] Based on laboratory observations of the aqueous fate of HPMTF, hydrolysis and ozonolysis drive the loss of HPMTF and primarily lead to sulfate formation rather than re-emission of OCS or SO_2.[10] These experiments were done under controlled laboratory parameters at elevated ozone conditions (60−80 ppb compared to 30 ppb) and neutral pH, which are atypical of the marine environment. While laboratory observations help isolate end products under controlled, extreme atmospheric conditions, they do not necessarily reflect the complexity and variability of oxidative conditions within the marine environment.

Here we use airborne in situ measurements of DMS and HPMTF, along with observational constraints on the oxidative environment and cloud properties, to assess the factors controlling HPMTF cloud loss within the marine boundary layer. Measurements were made off the coast of California under different conditions, including both clear skies and a stratocumulus cloud deck, as part of the Atmospheric Emissions and Reactions Observed from Megacities to Marine Areas (AEROMMA) campaign in June 2023.[17] The reactive uptake of HPMTF, as well as a constraint for the hydrolysis rate constant for HPMTF, was calculated for cloud droplets. Implications of the interplay between the transformation of HPMTF via hydrolysis or ozonolysis are evaluated to better understand the role of HPMTF in modulating the distribution of SO_2 and OCS in the marine boundary layer environment.

2. METHODS AND MATERIALS

2.1. Measurements of Gas-Phase Sulfur Made during the AEROMMA Campaign

Aircraft observations of key sulfur species throughout the sulfur oxidative pathway (e.g., DMS, HPMTF) were made from the NASA DC-8 suite of research instruments. In situ measurements were taken in the marine boundary layer off the coast of California under clear-sky and various cloud types during the AEROMMA campaign in June 2023.[17] From June 16−23, 2023 (DOY 167 −174), four research flights were conducted over the Pacific Ocean (Figure S1).

Hydroperoxymethyl thioformate (HPTMF) is detected using an iodide-adduct time-of-flight chemical ionization mass spectrometer (iodide CIMS, Aerodyne Research, Inc.).[5,18,19] Briefly, iodide ($[I]^-$) and iodide-water ($[I\cdot(H_2O)_n]^-$) ions cluster with ambient gases to form a stable iodide adduct ion ($[I\cdot M]^-$) that is detected via time-of-flight mass spectrometry (ToF-MS). Ambient air is sampled through a pressure-controlled (150 mbar), mass-flow-controlled (6 standard liters per min, SLPM) perfluoroalkoxy alkane (PFA) inlet (147 cm length, 0.64 cm ID), heated to 40 °C. The latter 55 cm of the inlet is heated to 130 °C to allow for the dissociation and detection of acyl peroxy nitrates (PANs). Water is dynamically added (via a saturated small N_2 flow, 0−100 sccm) directly into the ion−molecule reaction region (IMR) to maintain a consistent $[I]^-$:$[I\cdot(H_2O)_n]^-$ cluster ratio (ranging from 0.5−0.6), providing real-time compensation for changes in ambient humidity to maintain constant detection sensitivity. The IMR is maintained at a pressure of 40 mbar and 30 °C to reduce the effects of secondary ion chemistry and maintain constant detection sensitivity.[5,18] Instrument sensitivity and performance are evaluated throughout the campaign via standard additions of formic acid ($[I\cdot HCOOH]^-$; m/z 172.91) from a custom-calibrated permeation source and a continuously added ^{13}C isotopically labeled PAN (13C PAN), measured at both the carboxylate anion ($[^{13}C_2H_3O_2]^-$; m/z: 61.02) and the peroxy radical cluster ($[I\cdot^{13}C_2H_3O_3]^-$; m/z: 203.92), at the aircraft inlet. The HCOOH permeation source output is sampled every hour during flight on nitrogen zeros and is calibrated by a total carbon measurement.[20]

Dimethyl sulfide (DMS) is measured using a Vocus proton-transfer-reaction time-of-flight mass spectrometer (PTR-ToF-MS).[21] Dimethyl sulfoxide (DMSO) is detected by an ammonium-adduct long time-of-flight chemical ionization mass spectrometer (NH_4^+-LToF-CIMS).[22] The PTR-ToF-MS and NH_4^+-LToF-CIMS sampled air through a 40 °C, 1 m Teflon inlet at a maximum flow rate of 2 L min^{-1}. Instrument backgrounds were determined every 20 to 30 min by passing ambient air or zero-grade air through a platinum catalyst heated to 350 °C. The instruments were regularly calibrated at the beginning of each flight using multicomponent certified gas standards (Apel-Reimer). DMS was calibrated both in flight and after the campaign using a calibrated cylinder, and DMSO by an in-house liquid calibration source.

2.2. Calibration of Hydroperoxymethyl Thioformate

The sensitivity of the iodide CIMS to HPMTF was determined by the unit conversion of HPMTF from DMS oxidation using either chloride (Cl·) or nitrate radicals (NO_3·) as an oxidant. NO_3· and Cl· were used as the oxidant instead of OH, the dominant oxidant in the marine atmosphere, due to their selectivity for hydrogen abstraction rather

Downloaded from pubs.acs.org/aeacd5/article-pdf/doi/10.1021/acsestair.6c00199/6868709/acsestair.6c00199.pdf by UNIV OF YORK user on 06 October 2026

https://doi.org/10.1021/acsestair.6c00199
ACS EST Air XXXX, XXX, XXX−XXX

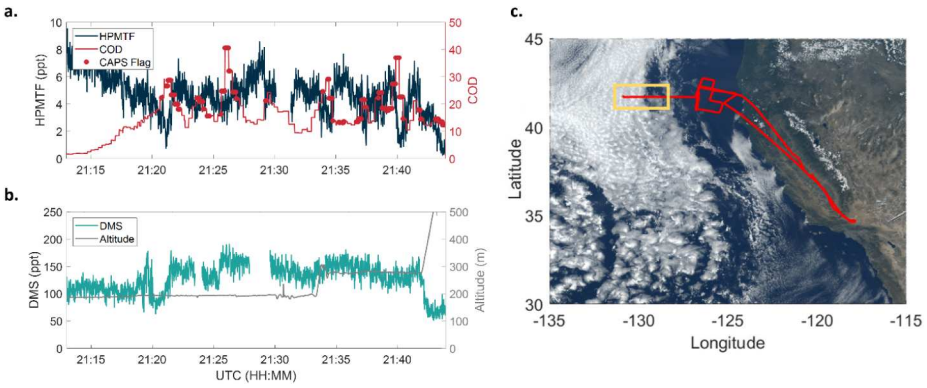


Figure 2. Time series of chemical measurements from the DC-8, taken during research Flight 3 (June 21, 21:00–22:00, 2023). 1-s time resolution of (a) HPMTF mixing ratio (dark-blue trace), cloud optical depth (COD, red trace), and instances when the CAPS detects a cloud droplet (red circles), (b) DMS mixing ratio (green trace), DC-8 altitude (gray trace). (c) True color image of flight path during AEROMMA June 21st 2023; yellow box indicates area highlighted in panels (a) and (b).

than addition at high temperatures.[23−25] These radicals preferentially produce the methyl thiomethyl peroxy radical (MTMP), the precursor to HPMTF (Figure 1). All experiments were performed under excess DMS (0.8−3 ppm) to ensure that NO_3· and Cl· preferentially react with DMS rather than other species within the reaction vessel (e.g., Cl·, RO_2·, HPMTF). An OH scavenger (carbon monoxide or propane) was added to the reaction vessel to consume any OH generated from the isomerization of MTMP, forming HPMTF (Figure 1).[24,26] Unaccounted OH could preferentially react with excess DMS, generating additional MTMP and HPMTF, leading to a nonquantitative relationship between NO_3·/Cl· consumed and HPMTF produced. Lastly, the calibrations were performed under higher temperatures (110−130 °C) to increase the isomerization rate, reduce adduct formation with Cl, and suppress competition from bimolecular reactions (e.g., MTMP + RO_2·, MTMP + NO_3·).[24] The culmination of these parameters allows for all oxidative radicals (NO_3· and Cl·) generated in the reaction vessel to react primarily with DMS, forming HPMTF. Under this assumption, we determined that the concentration of HPMTF measured by the CIMS is directly related to that of the generated radical concentrations (NO_3· and Cl·). The NO_3· and Cl· concentrations were determined by cavity ring-down spectroscopy and a Cl_2 laser photolysis equation described in sections S1 and S2 of the SI, respectively. To account for changes in the cluster ratio and temperature throughout the research flights, HPMTF sensitivity was calculated under various IMR temperatures (25−35 °C) and cluster ratios (0.4−0.65). Additional information on the experimental design is addressed in the SI (Sections S1−2, Figure S2).

2.3. Measurements of Ambient Aerosol and Cloud Properties

A 5-chan CPC (N-MASS),[27] Ultra-High Sensitivity Aerosol Size Spectrometer (UHSAS),[28] and Coarse-Mode Aerosol Size Spectrometer (CMASS) were utilized to calculate the dry (<40% RH) aerosol size distribution from 2.83 to 3178 nm.[29] Dry size distributions across the instrumentation were merged using a nonlinear inversion algorithm—a technique previously reported in detail by Brock et al. (2019) for a similar data set from the Atmospheric Tomography Mission (ATom) campaign. Accounting for aerosol hygroscopic growth due to high ambient RH (86 ± 4% RH), we assumed that most of the aerosol particles are sea spray and applied a growth factor of 2 to the aerosol distribution.[30] A total ambient aerosol surface area density was calculated by summing the surface areas of all particles across all bin sizes. The calculation uses the reported midpoint diameter for each size bin based on the aerosol ICARTT data file.

To identify areas of cloud influence and presence, a satellite-derived cloud optical depth (COD) and cloud top pressure (CTP) (GOES-West, www.star.nesdis.noaa.gov) were used. COD and CTP act as a proxy for cloud cover and fraction, respectively, while providing a near-real-time (5 min), spatially resolved (2 km resolution) approximation for when the research aircraft (DC-8) was sampling under clear-sky and cloudy conditions. To evaluate instances when the DC-8 was flying within a cloud, the second-generation cloud, aerosol, and precipitation spectrometer (CAPS) was used.[31] The CAPS consists of two main instruments: the Cloud and Aerosol Spectrometer (CAS) and the Cloud Imaging Probe (CIP), allowing for the quantification of particle and cloud droplet numbers and size distributions between approximately 0.5 and 50 μm.[31]

3. RESULTS AND DISCUSSION

3.1. Observations of Cloud Loss during a Stratocumulus Flight

Here, we present determinations of cloud loss within the marine environment for major species in the marine sulfur cycle—DMS, DMSO, and HPMTF—based on in situ measurements. The observed DMS/HPMTF ratio provides a metric for the loss of HPMTF relative to a given concentration of its precursor, DMS.[4,5,16] The DMS/HPMTF ratio can be expressed in terms of production and loss processes from a rearrangement of a steady-state approximation for HPMTF (i.e., d[HPMTF]/dt = 0), DMS/HPMTF was used to evaluate the current understanding of HPMTF loss under clear-sky and cloudy conditions. The steady-state approximation for HPMTF is used given the relatively fast ambient loss rate of HPMTF at midday, ranging from 11 h to <2 h under clear-sky and cloud conditions, respectively.[4,10] Generally, the DMS/HPMTF ratio tracks the relative loss of HPMTF, with elevated ratios indicating times of increased HPMTF loss. The steady-state DMS/HPMTF ratio can be expressed as (eq 1):

$$\frac{DMS}{HPMTF} = \frac{L_{OH} + L_{Aerosol} + L_{Dep} + L_{Res}}{P_{HPMTF}} \quad (1)$$

Here, DMS and HPMTF are the observed concentrations (ppt), P_{HPMTF} is the production of HPMTF from the OH oxidation of DMS (s^{-1}), and L_{OH}, $L_{Aerosol}$, and L_{Dep} are the loss of HPMTF via OH oxidation, aerosol uptake, and dry deposition, respectively (s^{-1}). L_{Res} is the residual loss of HPMTF due to other processes, such as photolysis and cloud uptake (s^{-1}). The analysis below takes this term to arise predominantly from cloud uptake. Across the four research flights, a tight correlation (R^2 = 0.74) was observed between DMS and HPMTF with a DMS/HPMTF median and interquartile range of 16.7 (13.7−19.4) across all clear-sky conditions (COD < 1 and CTP = Not a Number, NaN) (Figure S3c). We assume clear-sky conditions correspond to

Downloaded from pubs.acs.org/aeacd5/article-pdf/doi/10.1021/acsestair.6c00199/6868370/acsestair.6c00199.pdf by UNIV OF YORK user on 06 October 2026

https://doi.org/10.1021/acsestair.6c00199
ACS EST Air XXXX, XXX, XXX−XXX

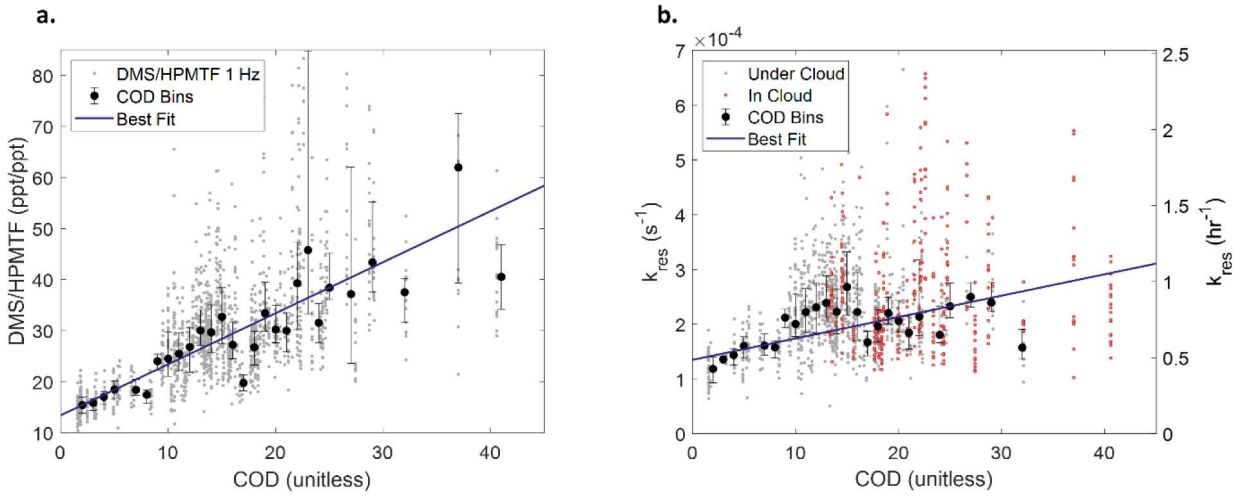


Figure 3. (a) 1-s resolution (gray), median (black dot), and interquartile range (error bar) of the DMS/HPMTF ratio values during the time under cloud, binned by whole cloud optical depth (COD) values. The blue line represents a best fit of the observations using a linear ODR (R^2 = 0.76). (b) 1-s-resolution observations of the calculated k_{res} (using eq 2) at varying COD. Observations are separated by under-cloud (gray) or in-cloud (red) using the CAPS probe. Median under-cloud and in-cloud binned observations (black circles), interquartile ranges (error bars), and an ODR best fit (blue line, R^2 = 0.55) are calculated using the same bins as (a).

times where HPMTF loss is driven by OH oxidation, deposition, photolysis, and aerosol uptake. If OH oxidation was the only driving loss process under clear-sky conditions, the observed DMS/HPMTF ratio, constrained by observations, would average 3.8 (±0.3). A ratio around 4 is observed during the AEROMMA marine flights, most prominently during the flight on 06/23/2023 (Figure S 3d), and indicates times over the marine atmosphere where the fate of HPMTF is driven primarily by OH oxidation. The elevated ratio across the campaign highlights the complexity and significant influence of HPMTF loss processes within the air masses.

Quantifying cloudy conditions and its role in HPMTF loss is complicated by cloud properties and types (i.e., optical thickness, cloud cover fraction, and cloud-base height) and coupling between the boundary layer and the cloud deck (i.e., cloud entrainment) not extracted from COD/CTP observations. There was no consistent or universal relationship between COD and DMS/HPMTF across the four research flights, indicating that COD alone is not a useful indicator of HPMTF cloud loss (Figure S4). Rather than identifying a universal relationship for approximating HPMTF loss, COD is used to target regions of elevated cloud cover for additional analysis. A correlation between COD and HPMTF is best seen during a section of research Flight 3 on June 21, 2023 (Figure 2a). Generally, Flight 3 proceeded by: 1) flying under clear-sky conditions; 2) stepping through various altitudes under a stratocumulus cloud deck (yellow-boxed area, Figure 2c); and 3) retracing previously sampled clear-sky conditions. DMS concentrations remained relatively constant (127 ± 27 ppt) throughout the portion of the flight (Figure 2b) along with wind speed and the steady-state-derived [OH] (explained further in Section 3.2),[32] implying that the primary production and "clear-sky" loss channels of HPMTF remained constant.

Under the stratocumulus cloud deck, an inverse relationship between cloud optical depth and HPMTF concentrations is observed (Figure 2 and Figure S5), consistent with an HPMTF loss to clouds.[4,12,16] In addition to the satellite-derived metric for cloud cover, an in situ cloud indicator (measured by the CAPS system) highlighted instances of elevated HPMTF loss when the DC-8 flew through and around clouds within the boundary layer (red circles; Figure 2b). A positive correlation (R^2 = 0.76) is observed when the DMS/HPMTF ratio (approximating the instantaneous loss of HPMTF; eq 1) is regressed against COD across this portion of the flight (Figure 3a). Additionally, the linear orthogonal distance regression (ODR) intercept of the DMS/HPMTF regression (Figure 3a) within the cloudy region is 14.1 ± 1.2. This intercept falls within the uncertainty of the campaign median DMS/HPMTF, 16.7 (13.7−19.4), for clear-sky conditions (COD < 1 and CTP = NaN). Lastly, the air mass sampled before entering the cloud deck observed a DMS/HPMTF ratio of ∼5 (Figure S6b). The increase in DMS/HPMTF (driven by HPMTF loss) from an OH-only-driven ratio (∼4) to a sustained elevated ratio (∼16) can be attributed to past and current interactions with marine clouds. The positive correlation highlights the role of cloud uptake as an important sink of HPMTF within the boundary layer as clouds have large aqueous surfaces that have been shown to irreversibly react with HPMTF.[10,11,16] Research Flight 3 will be used as a test case for understanding cloud interactions of reactive gases under consistent precursor concentrations. To quantify the loss of HPMTF to cloud droplets, we target sampling within thin, dispersed clouds and assume the steady-state approximation for HPMTF when sampling through the dispersed cloud decks. The dispersed cloud decks result from a unique boundary layer facilitating the formation of thin clouds under a thick stratocumulus cloud deck (Figure S7). The thin clouds provide a unique opportunity to investigate the interaction of HPMTF with cloud droplets while mitigating the potential for HPMTF titration observed within thick cloud decks.[4,16]

3.2. Drivers of HPMTF Loss within a Thin Cloud Deck

HPMTF is a highly soluble/reactive species whose irreversible uptake and fast gas diffusion rate to the cloud result in short in-cloud lifetimes (<5 s), supporting the use of the steady-state approximation within cloud-influenced areas.[4,33] To approximate the first-order loss rate coefficient of HPMTF to clouds, the steady-state approximation, eq 1, is rearranged and expanded to solve for the residual loss term (eq 2):

Downloaded from pubs.acs.org/aeacd5/article-pdf/doi/10.1021/acsestair.6c00199/6868709/acsestair.6c00199.pdf by UNIV OF YORK user on 06 October 2026

https://doi.org/10.1021/acsestair.6c00199
ACS EST Air XXXX, XXX, XXX−XXX

$$k_{res} = \frac{[DMS]}{[HPMTF]} f_{isom} k_{OH,Abs}[OH] - \left(\frac{r_{aer}}{D_g} + \frac{4}{w \cdot \gamma_{aer}}\right)^{-1} S_A - \frac{v_d}{BLH} - k_{OH,HPMTF}[OH] \quad (2)$$

where $[DMS]$ is the measured ambient DMS concentration (units of molec. cm^{-3}), $[HPMTF]$ is the measured ambient HPMTF concentration (units of molec. cm^{-3}), D_g is the diffusivity of HPMTF (units of $cm^2\ s^{-1}$) in air using the additive "Schroeder" method,[34] r_{aer} is the measured Sauter mean aerosol radius (units of cm),[28,29] ω is the mean molecular speed of HPMTF (units of cm s^{-1}), γ_{aer} is the unitless reactive uptake coefficient corresponding to an experimentally measured value for deliquesced NaCl particles,[9] S_A is the measured ambient aerosol surface area density (units of $cm^2\ cm^{-3}$), v_d is a wind-speed-dependent dry deposition velocity (units of cm s^{-1}),[4,12,35] BLH is the marine boundary layer height calculated from inflection points in potential temperature and water mixing ratio during DC-8 altitude profiles (units of cm), $k_{OH,HPMTF}$ is the HPMTF+OH rate constant (1.4×10^{-11} cm^3 $molec^{-1}$ s^{-1}),[10] [OH] is the ambient OH concentration (units of molec. cm^{-3}) calculated from eq 3, k_{res} is the residual or unconstrained first-order loss rate constant added to account for any additional reactions missing in the analysis (e.g., cloud loss, error in loss terms, artificial loss because not as steady state), $k_{OH,Abs}$ is the temperature-dependent hydrogen abstraction rate constant (units of cm^3 $molec^{-1}$ s^{-1}) for DMS,[23] and f_{isom} is the fraction of MTMP that yields HPMTF. The f_{isom}term accounts for the competition of MTMP between isomerization (that forms HPMTF) and bimolecular chemistry with NO, HO_2, and RO_2 (calculation of f_{isom} is described in SI Appendix, section S3; Figure S3a). The hydroxyl radical concentration, [OH], is calculated through a steady-state approximation represented in eq 2:

$$[OH] = \frac{fO(1D) \cdot jO_3 \cdot [O_3] \cdot 2 + k_{NO+HO_2}[NO][HO_2]}{OHR} \quad (3)$$

where $fO(1D)$ is the fraction of produced $O(^1D)$ reacting with water vapor, jO_3 is the observed first-order photolysis rate of ozone yielding $O(^1D)$ (units of s^{-1}),[36] $[O_3]$ is the ambient ozone concentration (units of molec. cm^{-3}),[37] [NO] is the measured ambient nitric oxide concentration (units of molec. cm^{-3}),[38] $[HO_2]$ is the ambient hydroperoxyl radical concentration set to 2.6×10^8 (~10 ppt) (Figure S3b), and OHR is the measured OH reactivity (units of s^{-1}).[39] Additional information on the calculation of $[HO_2]$ and [OH] using steady-state approximations is described in sections S4 and S5 and Figure S8 of the SI.

The residual loss (k_{res}) is directly proportional to the DMS/HPMTF ratio calculated and modulated by the relative loss pathways of HPMTF at the time of sampling (eq 2). The residual loss calculated during this section of the research flight accounts for changes in oxidative (e.g., [OH], NO) and environmental parameters (e.g., wind speed, photon flux) and assumes to reflect cloud loss due to interaction in and around a cloud deck. As explained in section 3.1, the regression of the cloud optical depth to the DMS/HPMTF ratio indicated a y-intercept similar to that of cloud-influenced conditions during the entire AEROMMA campaign. A positive moderate correlation (R^2 = 0.55) between the COD and the residual loss is observed as the DC-8 flies under the stratocumulus cloud deck (Figure 3). While within the cloud sampling, consistent observed winds (7.16 ± 0.64 m/s) and aerosol surface area (152 ± 26 μm^2 cm^{-3}), measured between 3 nm and 3 μm [29], contribute only 1.4% and 5.6%, respectively, to the overall noncloud loss processes of HPMTF, indicating that the observed DMS/HPMTF ratio is primarily driven by OH oxidation and cloud loss (Figure S9). Calculated loss and production processes of HPMTF (e.g., OH-driven production, aerosol loss, and deposition) remain relatively constant across the flight path, highlighting that variability in calculated k_{res} is driven by the presence of clouds and not changes in constrained parameters (Figure S9). As discussed earlier, the COD inversely tracks with the photon flux and in situ observations of the first-order photolysis rates of NO_2 and O_3 (Figure S10). The decrease in ozone photolysis as a function of cloud fraction will lead to a corresponding decrease in the instantaneous production of OH through the O(1D) production channel (Figure S10c). With minimal changes in O_3, H_2O and temperature, and low NO, the observed decrease in steady-state [OH] is driven by the O_3 photolysis rate (Figure S10). The decreasing [OH] should not drive the observed increase in k_{res} due to the assumed elevated OH loss rates of HPMTF compared to DMS. While the temperature dependence of the OH rate constant for HPMTF has not been measured, the room-temperature OH rate constant of HPMTF is 3 times faster than that of the DMS hydrogen abstraction channel that generates HPMTF. The faster OH loss of HPMTF and relatively constant DMS concentration would lead to an overall decrease in the DMS/HPMTF ratio at higher COD/lower relative OH, contrary to what is observed in Figure 3. For this reason, we assume the temporal HPMTF structure and calculated residual loss is associated with cloud processing. In contrast to the positive correlation between COD and HPMTF loss, DMSO, a key stable intermediate from the OH-addition channel of DMS oxidation (Figure 1) and produced at a similar rate as HPMTF,[23] shows a negative correlation with respect to the observed COD (Figure S11). The DMS/DMSO ratio shows a negative correlation, matching the calculated OH trend (Figure S10c), implying that the driver of DMSO loss, even under cloudy conditions, is still OH oxidation (9.6×10^{-11} cm^3 $molec^{-1}$ s^{-1} at 290 K). If HPMTF loss across this section of the flight were dominated by OH, then HPMTF would show a trend akin to that observed by DMSO. The effect from OH + HPMTF under and within the cloud is still present and accounted ($-k_{OH,HPMTF}[OH]$ in eq 2), but the cloud uptake is simply larger and dominates the observed changes in k_{res}.

3.3. Reactive Uptake of HPMTF to Cloud Droplets

The relationship between k_{res} and COD seems to fall into two groups corresponding to under-cloud and in-cloud sampling (red circles, Figure 3a). In-cloud sampling is identified utilizing the CAPS probe, which is equipped with an optical spectrometer that measures cloud properties. All other points are taken to be under the cloud deck, verified visually with the front facing camera and by relating the DC8 altitude to a MERRA-2[40] reanalysis product of vertically resolved cloud fraction (Figure S7). The gradual increase in the residual loss term as a function of the COD until a COD value of approximately 15 could indicate an HPMTF loss term that is dependent on the fraction and depth of the above-cloud deck. A relatively constant first-order residual loss is observed for points above a COD of 15 and flagged as in-cloud, with a

Downloaded from pubs.acs.org/aeacd5/article-pdf/doi/10.1021/acsestair.6c00199/6868709/acsestair.6c00199.pdf by UNIV OF YORK user on 06 October 2026

https://doi.org/10.1021/acsestair.6c00199
ACS EST Air XXXX, XXX, XXX−XXX

median and interquartile range of 2.3 (1.8−3.1) × 10^{-4} s^{-1} (Figure 3). While in-cloud, the driving residual loss process should be diffusion and uptake to cloud droplets. This process of HPMTF reactive uptake to cloud droplets can be written as the following equation:

$$k_{res} = SA_{cld}\left(\frac{r_{cld}}{D_g} + \frac{4}{w\cdot\gamma_{Cld}}\right)^{-1} \quad (4)$$

where SA_{cld} is the cloud droplet surface area concentration (units of cm^2 cm^{-3}), r_{cld} is the average mean radius of the cloud distribution within the sample air mass (units of cm), D_g is the gas-phase diffusion of HPMTF (units of cm^2 s^{-1}), ω is the mean molecular speed of HPMTF (units of cm s^{-1}), and γ_{cld} is the reactive uptake of HPMTF to cloud droplets. A median and interquartile range of 373 (252−488) μm^2 cm^{-3} and an approximated value of 5 μm were observed for the cloud surface area and radius, respectively. These values fall within the range of previous observations made for stratocumulus clouds.[41]

Constrained by observations made from the CAPS probe, we calculate a reactive uptake coefficient of HPMTF to cloud droplets of 1.2 (0.9−1.9) × 10^{-2}. The observed value falls in between values calculated for HPMTF onto dry NaCl (1.9 ± 1.3) × 10^{-4}, wetted NaCl (1.6 ± 0.6 × 10^{-3}) and wetted NaI (0.72 ± 0.14) aerosols.[9] As discussed by Jernigan et al. (2022), the composition and aqueous nature of the aerosol influence the relative HPMTF loss. The value observed matches the approximated value used in recent publications constraining HPMTF's loss to cloud droplets in climate models.[4,6,9]

3.4. Aqueous First-Order Loss Rate of HPMTF

To understand the drivers of reactive uptake variability, the following equation from Hanson et al., 1994 is used:[42]

$$\frac{1}{\gamma_{Cld}} = \frac{1}{\alpha} + \frac{w}{4HRT\sqrt{k_{aq}D_l}\left[\coth\left(\frac{r_{cld}}{l_{RD}}\right) - \frac{l_{RD}}{r_{cld}}\right]} \quad (5)$$

where γ_{cld} is the reactive uptake of HPMTF to cloud droplets (unitless), α is the mass accommodation factor for HPMTF (unitless), H is the Henry's law coefficient (units M atm^{-1}), ω is the mean molecular speed of HPMTF (units of cm s^{-1}), R is the ideal gas constant (units of atm M^{-1} K^{-1}), T is the ambient temperature (units of K), D_l is the aqueous-phase diffusion of HPMTF using the Wilke−Chang equation (units of cm^2 s^{-1}),[43] k_{aq} is the overall first-order aqueous loss rate coefficient of HPMTF (units of s^{-1}), r_{cld} is the cloud droplet radius (units of cm), and l_{RD} is the reacto-diffusive depth ($l_{RD} = \sqrt{D_l/k_{aq}}$, units of cm). While Henry's law and mass accommodation values of HPMTF have not been measured, approximations using structure−activity relationships, values for similar sulfur species, and previous measurements can provide constraints on the range in values for the first-order aqueous loss rate of HPMTF in cloud droplets. Figure 4 shows the range in potential overall first-order aqueous loss rates of HPMTF at various Henry's law and mass accommodation values.

Reactions on larger droplets can have mass-transport and diffusion limitations, controlling the possible observable HPMTF aqueous loss rates. The limitations in observable HPMTF aqueous loss rates at given cloud droplet diameters are presented in Figure S12. To limit the maximum observable

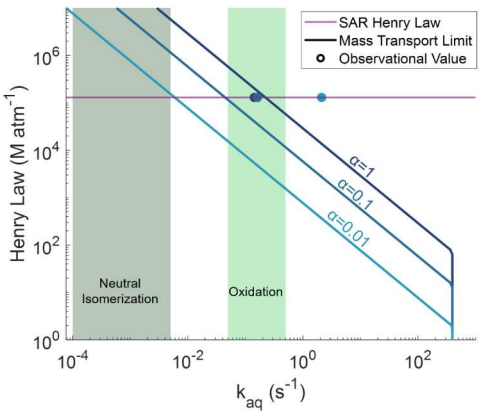


Figure 4. Range in overall first-order aqueous loss rate constant of HPMTF (k_{aq}, s^{-1}) as a function of a range of Henry's law coefficients. The purple line represents the approximated Henry's law coefficient for HPMTF using a structure activity relationship (1.3 × 10^5 M atm^{-1}). The blue traces represent the maximum first-order aqueous loss rate given mass-transport limitations of HPMTF to the droplet at a given mass accommodation value with the darker and lighter hues representing the upper bound (1) and lower bound (0.012), respectively. The shaded regions provide ranges of hydroperoxy-aldehyde isomerization values in neutral solution (dark green) and DMS oxidation by ozone and hydrogen peroxide (light green). Median retrieved overall first-order aqueous loss rate constant of HPMTF at a Henry's law constant of 1.3 × 10^5 and mass accommodation of 1, 0.1, and 0.012 are presented as circles of darker to lighter hues of blue, respectively. All points are calculated using an average cloud droplet diameter of 10 μm.

first-order aqueous rate constant, the following equation outlined in Seinfeld and Pandis is used:[44]

$$k_{aq}H \le \varepsilon\frac{3\alpha}{r_{cld}\sqrt{2\pi RTM_A}} \quad (6)$$

where ε is a unitless, arbitrary value set to 0.1, indicating no interfacial mass-transport limitations, and M_A is the molecular weight of HPMTF (units of kg mol^{-1}). The maximum possible observable aqueous rate, shown as blue lines in Figure 4, depends on the cloud droplet radius (5 μm) and the assumed mass accommodation coefficient. This upper bound dictates that first-order aqueous loss rates above that line are indistinguishable and limited by the rate HPMTF can diffuse to the cloud droplet. The mass accommodation value needs to be greater than 0.01 to explain the observed reactive uptake. Given the highly functionalized nature of HPMTF, its mass accommodation could be 0.01, 0.1, and 1, corresponding to values of the similar functionalized methyl hydroperoxide (MHP), DMSO, and HPMTF onto wetted NaI aerosol, respectively.[9,45,46] While a mass accommodation value greater than 0.72 is needed to explain the observed reactive uptake of HPMTF onto NaI aerosols, we assume that the value for HPMTF for the rest of the analysis to be 0.1, typical of other soluble sulfur compounds (e.g., DMSO, MSA, SO_2).[45,47] The analysis for determining the calculated aqueous loss rate of HPMTF in clouds is insensitive to values greater than 0.1, and the large value for HPMTF observed in the NaI aerosol experiments could be due to properties of the generated aerosol atypical to ambient conditions and cloud droplets (e.g., high ionic strength and surface activity of I^-).

Henry's law coefficient is also unknown for HPMTF, but its value can be approximated and constrained by structure−

Downloaded from pubs.acs.org/aeacd5/article-pdf/doi/10.1021/acsestair.6c00199/6868370/acsestair.6c00199.pdf by UNIV OF YORK user on 06 October 2026

https://doi.org/10.1021/acsestair.6c00199
ACS EST Air XXXX, XXX, XXX−XXX

activity relationships and molecules with similar functional groups. The HPMTF's Henry' law constant was estimated to be 1.3×10^5 and 1.3×10^4 M atm^{-1} using a bond contribution method and Vapor Pressure/Water Solubility (VP/WSOL), respectively.[48,49] While the Vapor Pressure/Water Solubility method is reliable with sufficient experimental data, HPMTF does not have a known vapor pressure or water solubility, and as such, this method is as uncertain as the bond contribution method. With few measured Henry's law values for hydroperoxides, large assumed HPMTF solubility, and multiple functional groups within HPMTF, the relative error and uncertainty of the calculated value increase (3 hydroperoxides, 10^3 M atm^{-1}, >2 functional groups).[48,50] Even so, the approximated Henry's law matches with measured values from other highly functionalized hydroperoxides (ISOPOOH, 1.18×10^5 M atm^{-1}) and sulfur compounds (DMSO, 9×10^5 M atm^{-1}).[51] Under the assumptions and large uncertainty, we estimate Henry's law for HPMTF to be 1.3×10^5 M atm^{-1}.

Using a mass accommodation of 0.1 and a Henry's law of 10^5 M atm^{-1}, we estimate the overall first-order aqueous loss rate constant of HPMTF within the cloud droplet is 1.4 (0.4−2.2) $\times 10^{-1}$ s^{-1}. The lower and upper limits of this rate are bounded by the mass-transport limitation of HPMTF at α of 0.1 and 1, respectively. While the 1.4×10^{-1} s^{-1} rate constant is faster than the maximum observable rate (0.5×10^{-1} s^{-1} at α of 0.1), we still recommend this value as the overall rate constant. The rate constant is relatively insensitive to a $\alpha > 0.1$, and the observation would be possible if α was 0.72, derived from the NaI aerosol experiments.[9] This rate constant dictates a reacto-diffusive length of 84 μm for HPMTF. The length is greater than the radius of the cloud droplet, allowing diffusion into the bulk of the cloud droplet, where a variety of different oxidative and hydrolysis-based mechanisms can compete.

3.5. Mechanisms Driving Aqueous Loss of HPMTF

Under the assumptions discussed earlier, we find that hydrolysis or oxidation of HPMTF (e.g., O_3, H_2O_2, SO_2) within cloud droplets are the likely loss paths that explain our derived first-order loss rate constant of 1.4 (0.4−2.2) $\times 10^{-1}$ s^{-1}. If HPMTF loss in the cloud droplet occurs through oxidation (e.g., O_3, OH), we propose HPMTF will rapidly and efficiently go on to form sulfate.[11] Alternatively, HPMTF hydrolysis, increased by particle acidity, has been proposed to lead to the formation of thioacids (R−C(=S)OH or R−C(=O)SH) or cyclic thioperhemiacetal.[11,13,52] If HPMTF oxidizes at the same rate as DMS via O_3 (30 ppb, 0.5 nM) and H_2O_2 (1 ppb, 80 μM), then the pseudo-first-order loss to these oxidants would be 0.2 and 0.03 s^{-1}, respectively.[53] Our derived rate constant falls within this range of oxidation-based reactions. Both DMS and HPMTF have a reduced sulfur atom within their structure and are the target for O_3 and H_2O_2 oxidation. Though HPMTF can diffuse into the bulk, we believe that neutral hydrolysis will not compete with other pathways, given its slower rate constants.[13,54] The rate of hydrolysis can be exponentially increased with increased acidity of the particle and cloud droplet, with a recent theoretical study calculating acid-catalyzed rate constants $\gg 1$ s^{-1} for HPMTF[13,52] Fast acid-catalyzed rate constants exceeded the mass-diffusion limit and are indistinguishable at any mass accommodation coefficient. In any case, the proposed result of hydrolysis is a thioperhemiacetal formed via an isomerization reaction which, like HPMTF, can undergo additional oxidation, eventually leading to the formation of sulfate.[11,52,55] In contrast, the thioperhemiacetal can further decompose into thioacids, providing a route for the re-emission of OCS and SO_2.[11,13] This is a deviation from the previous understanding of sulfate formation from the aqueous transformation of HPMTF that could provide a route for an overall increase in the SO_2 and OCS yield from DMS oxidation.[4,6,7,10]

4. CONCLUSIONS AND ATMOSPHERIC IMPLICATIONS

Here we present an observationally constrained value for HPMTF reactive uptake of 1.2 (0.9−1.9) $\times 10^{-2}$ which would translate to a first-order overall aqueous loss of 1.4 (0.4−2.2) $\times 10^{-1}$ s^{-1}. The observations made here are built on the assumption that the thin dispersed clouds sampled represented marine cloud droplets and that HPMTF was at steady-state when sampling through the dispersed cloud decks. The observed reactive uptake is an order of magnitude larger than the reactive uptake of HPMTF to wetted NaCl aerosols, highlighting the role of dissolved oxidants and acids in ambient cloud droplet, increasing HPMTF's loss. The observed reactive uptake matches the significant value used in current climate models (1.6×10^{-2}), reiterating the importance of cloud dynamics on HPMTF's fate.[4,11,16] We also present a positive correlation between cloud optical depth (COD) and the residual HPMTF loss within clouds (k_{res}), providing a link between a satellite retrieval product and the loss of a climate-relevant species. Though a correlation with COD is observed, cloud type and boundary layer dynamics also play an important role in the overall loss rate of soluble molecules.[15] Publications observing tightly coupled boundary layers[4] or in-cloud analysis (this study) help frame and evaluate the complexity and variability of the marine atmosphere and cloud-climate interactions. The observed DMS/HPMTF ratios of 16 found in this and previous work point to air masses consistently influenced by cloud processing and interactions.[4,16] This and recent work imply that the dominant fate of HPMTF after cloud uptake will likely be oxidation and the eventual formation of sulfate.[11,13] While hydrolysis could provide an efficient, initial, and irreversible loss of HPMTF within the cloud droplet, the presence of oxidants in the cloud should lead to the eventual formation of S(IV) via the oxidation of HPMTF hydrolysis products (e.g., thioacids). The lack of knowledge on the eventual role of the thioacids leaves uncertainty on this assumption, and future work focused on determining the condensed-phase mechanism that explores the competition between the formation of sulfate and HPMTF-derived thioacids would be of interest. A focus on the role of oxidants and acidity, as they are critical components of atmospheric aerosols and clouds, would provide further insight into the fate of HPMTF and sulfur processing over the marine environment. Lastly, the use of the cloud probe can be applied to other soluble species (e.g., HNO_3, SO_2, H_2O_2) to create an observational constraint on the role of clouds in regulating the oxidative environment in the marine atmosphere.[15]

■ ASSOCIATED CONTENT

Data Availability Statement

The data underlying this study are publicly available on the AEROMMA data archive:https://csl.noaa.gov/projects/aeromma/data.html.

Downloaded from pubs.acs.org/aeacd5/article-pdf/doi/10.1021/acsestair.6c00199/6868370/acsestair.6c00199.pdf by UNIV OF YORK user on 06 October 2026

https://doi.org/10.1021/acsestair.6c00199
ACS EST Air XXXX, XXX, XXX−XXX

Supporting Information

The Supporting Information is available free of charge at https://pubs.acs.org/doi/10.1021/acsestair.6c00199.

A description of HPMTF calibration, MTMP isomerization, HO_2 approximation, and the OH calculation is presented in the SI, along with supplemental figures referenced in the main text (PDF)

AUTHOR INFORMATION

Corresponding Author

Christopher M. Jernigan − *Cooperative Institute for Research in Environmental Sciences, University of Colorado Boulder, Boulder, Colorado 80309, United States; NOAA Chemical Sciences Laboratory, Boulder, Colorado 80305, United States;* Present Address: U.S. Environmental Protection Agency, Research Triangle Park, NC 27711, United States; orcid.org/0000-0003-0302-5222; Email: jernigan.chris@epa.gov

Authors

Gordon A. Novak − *NOAA Chemical Sciences Laboratory, Boulder, Colorado 80305, United States;* Present Address: Department of Chemistry, University of York, York, YO10 5DD, United Kingdom.

Siyuan Wang − *Cooperative Institute for Research in Environmental Sciences, University of Colorado Boulder, Boulder, Colorado 80309, United States; NOAA Chemical Sciences Laboratory, Boulder, Colorado 80305, United States;* Present Address: Department of Atmospheric Sciences, Rosenstiel School of Marine, Atmospheric, and Earth Science, University of Miami, Florida, 33124, United States.

Michael A. Robinson − *Cooperative Institute for Research in Environmental Sciences, University of Colorado Boulder, Boulder, Colorado 80309, United States; NOAA Chemical Sciences Laboratory, Boulder, Colorado 80305, United States;* orcid.org/0000-0003-0977-9148

Adam Ahern − *Cooperative Institute for Research in Environmental Sciences, University of Colorado Boulder, Boulder, Colorado 80309, United States; NOAA Chemical Sciences Laboratory, Boulder, Colorado 80305, United States;* orcid.org/0000-0003-3461-2673

Osinachi Ajoku − *Department of Earth, Environment and Equity, Howard University, Washington, D.C. 20059, United States*

Katherine Ball − *Division of Chemistry and Chemical Engineering, California Institute of Technology, Pasadena, California 91125, United States*

Timothy H. Bertram − *Department of Chemistry, University of Wisconsin−madison, Madison, Wisconsin 53706, United States;* orcid.org/0000-0002-3026-7588

Kelvin H. Bates − *Cooperative Institute for Research in Environmental Sciences, University of Colorado Boulder, Boulder, Colorado 80309, United States; NOAA Chemical Sciences Laboratory, Boulder, Colorado 80305, United States;* Present Address: Department of Mechanical Engineering, University of Colorado Boulder, Boulder, Colorado 80309, United States.

Birger Bohn − *Institute of Climate and Energy Systems, ICE-3: Troposphere, Forschungszentrum Jülich, Jülich 52428, Germany;* orcid.org/0000-0003-4177-3934

Charles A. Brock − *NOAA Chemical Sciences Laboratory, Boulder, Colorado 80305, United States*

Wyndom S. Chace − *Cooperative Institute for Research in Environmental Sciences, University of Colorado Boulder, Boulder, Colorado 80309, United States; NOAA Chemical Sciences Laboratory, Boulder, Colorado 80305, United States; Department of Chemistry, University of Colorado Boulder, Boulder, Colorado 80309, United States;* orcid.org/0009-0009-1951-2050

Matthew Coggon − *NOAA Chemical Sciences Laboratory, Boulder, Colorado 80305, United States;* orcid.org/0000-0002-5763-1925

Maximilian Dollner − *University of Vienna, Faculty of Physics, Aerosol Physics and Environmental Physics, Vienna 1090, Austria*

Michelle Färber − *Institute of Climate and Energy Systems, ICE-3: Troposphere, Forschungszentrum Jülich, Jülich 52428, Germany;* orcid.org/0009-0003-0302-6142

Zachary Finewax − *Cooperative Institute for Research in Environmental Sciences, University of Colorado Boulder, Boulder, Colorado 80309, United States; NOAA Chemical Sciences Laboratory, Boulder, Colorado 80305, United States;* Present Address: Colorado Department of Public Health and Environment, Air Pollution Control Division/ Air Toxics and Ozone Precursors Program, Wheat Ridge, Colorado 80033, United States.

Hendrik Fuchs − *Institute of Climate and Energy Systems, ICE-3: Troposphere, Forschungszentrum Jülich, Jülich 52428, Germany; Department of Physics, University of Cologne, Cologne 50937, Germany;* orcid.org/0000-0003-1263-0061

Georgios I. Gkatzelis − *Institute of Climate and Energy Systems, ICE-3: Troposphere, Forschungszentrum Jülich, Jülich 52428, Germany;* orcid.org/0000-0002-4608-3695

Han Huynh − *Cooperative Institute for Research in Environmental Sciences, University of Colorado Boulder, Boulder, Colorado 80309, United States; NOAA Chemical Sciences Laboratory, Boulder, Colorado 80305, United States;* orcid.org/0000-0002-2467-7134

Jan Kazil − *Cooperative Institute for Research in Environmental Sciences, University of Colorado Boulder, Boulder, Colorado 80309, United States; NOAA Chemical Sciences Laboratory, Boulder, Colorado 80305, United States;* Present Address: Blue Earth Analytics, Lafayette, CO, 80026, USA.

Ming Lyu − *Cooperative Institute for Research in Environmental Sciences, University of Colorado Boulder, Boulder, Colorado 80309, United States; NOAA Chemical Sciences Laboratory, Boulder, Colorado 80305, United States;* orcid.org/0000-0001-9746-0465

Anna Novelli − *Institute of Climate and Energy Systems, ICE-3: Troposphere, Forschungszentrum Jülich, Jülich 52428, Germany;* orcid.org/0000-0003-2077-7573

Jeff Peischl − *Cooperative Institute for Research in Environmental Sciences, University of Colorado Boulder, Boulder, Colorado 80309, United States; NOAA Chemical Sciences Laboratory, Boulder, Colorado 80305, United States;* Present Address: NOAA Global Monitoring Laboratory, Boulder, Colorado 80305, United States.; orcid.org/0000-0002-9320-7101

Downloaded from pubs.acs.org/aeacd5/article-pdf/doi/10.1021/acsestair.6c00199/6868370/acsestair.6c00199.pdf by UNIV OF YORK user on 06 October 2026

Andrew Rollins − *NOAA Chemical Sciences Laboratory, Boulder, Colorado 80305, United States;* orcid.org/0000-0002-1020-3966

Nell B. Schafer − *Cooperative Institute for Research in Environmental Sciences, University of Colorado Boulder, Boulder, Colorado 80309, United States; NOAA Chemical Sciences Laboratory, Boulder, Colorado 80305, United States; Department of Chemistry, University of Colorado Boulder, Boulder, Colorado 80309, United States;* orcid.org/0009-0000-2287-3775

Aaron Stainsby − *Institute of Climate and Energy Systems, ICE-3: Troposphere, Forschungszentrum Jülich, Jülich 52428, Germany*

Chelsea E. Stockwell − *NOAA Chemical Sciences Laboratory, Boulder, Colorado 80305, United States;* orcid.org/0000-0003-3462-2126

Patrick R. Veres − *NSF NCAR Earth Observing Laboratory, Boulder, Colorado 80307, United States*

Carsten Warneke − *NOAA Chemical Sciences Laboratory, Boulder, Colorado 80305, United States;* orcid.org/0000-0003-3811-8496

Eleanor Waxman − *Cooperative Institute for Research in Environmental Sciences, University of Colorado Boulder, Boulder, Colorado 80309, United States; NOAA Chemical Sciences Laboratory, Boulder, Colorado 80305, United States;* orcid.org/0000-0001-5045-8149

Bernadett Weinzierl − *University of Vienna, Faculty of Physics, Aerosol Physics and Environmental Physics, Vienna 1090, Austria*

Kevin Wokosin − *Department of Chemistry, University of Wisconsin−madison, Madison, Wisconsin 53706, United States;* orcid.org/0000-0002-4740-1173

Lu Xu − *Cooperative Institute for Research in Environmental Sciences, University of Colorado Boulder, Boulder, Colorado 80309, United States; NOAA Chemical Sciences Laboratory, Boulder, Colorado 80305, United States;* Present Address: Department of Energy, Environmental, and Chemical Engineering, Washington University in St. Louis, St. Louis, Missouri 63130, United States.; orcid.org/0000-0002-0021-9876

Kristen Zuraski − *Cooperative Institute for Research in Environmental Sciences, University of Colorado Boulder, Boulder, Colorado 80309, United States; NOAA Chemical Sciences Laboratory, Boulder, Colorado 80305, United States;* Present Address: Quantinuum, Broomfield, CO, 80021, United States.

Steven S. Brown − *NOAA Chemical Sciences Laboratory, Boulder, Colorado 80305, United States; Department of Chemistry, University of Colorado Boulder, Boulder, Colorado 80309, United States; Division of Geological and Planetary Sciences, California Institute of Technology, Pasadena, California 91125, United States;* orcid.org/0000-0001-7477-9078

Complete contact information is available at: https://pubs.acs.org/10.1021/acsestair.6c00199

Notes

The authors declare no competing financial interest.

■ ACKNOWLEDGMENTS

C.M.J., S.W., M.A.R., A.A., K.H.B., W.S.C., Z.F., H.H., J.K., J.P., N.B.S., E.W., L.X., and K.Z. were partially supported by the NOAA Cooperative Agreement with CIRES, NA22OAR4320151. The authors acknowledge Paul Wennberg and John Crounse for their comments on the analysis, as well as their ambient measurements of H_2O_2 used to validate the HO_2 mixing ratio approximation.

■ REFERENCES

(1) (a) Lana, A.; Bell, T.; Simó, R.; Vallina, S. M.; Ballabrera-Poy, J.; Kettle, A.; Dachs, J.; Bopp, L.; Saltzman, E.; Stefels, J.; et al. An updated climatology of surface dimethlysulfide concentrations and emission fluxes in the global ocean. *Global Biogeochem. Cycles* **2011**, *25* (1), 1004. (b) Galí, M.; Levasseur, M.; Devred, E.; Simó, R.; Babin, M. Sea-surface dimethylsulfide (DMS) concentration from satellite data at global and regional scales. *Biogeosciences* **2018**, *15* (11), 3497−3519.

(2) Vallina, S. M.; Simó, R.; Anderson, T. R.; Gabric, A.; Cropp, R.; Pacheco, J. M. A dynamic model of oceanic sulfur (DMOS) applied to the Sargasso Sea: Simulating the dimethylsulfide (DMS) summer paradox. *J. Geophys. Res.: Biogeosci.* **2008**, *113* (G1), G01009.

(3) (a) Crutzen, P. J. The possible importance of CSO for the sulfate layer of the stratosphere. *Geophys. Res. Lett.* **1976**, *3* (2), 73−76. (b) Solomon, S.; Garcia, R. R.; Rowland, F. S.; Wuebbles, D. J. On the depletion of Antarctic ozone. *Nature* **1986**, *321* (6072), 755−758. (c) Asaf, D.; Rotenberg, E.; Tatarinov, F.; Dicken, U.; Montzka, S. A.; Yakir, D. Ecosystem photosynthesis inferred from measurements of carbonyl sulphide flux. *Nat. Geosci.* **2013**, *6* (3), 186−190.

(4) Novak, G. A.; Fite, C. H.; Holmes, C. D.; Veres, P. R.; Neuman, J. A.; Faloona, I.; Thornton, J. A.; Wolfe, G. M.; Vermeuel, M. P.; Jernigan, C. M.; et al. Rapid cloud removal of dimethyl sulfide oxidation products limits SO2 and cloud condensation nuclei production in the marine atmosphere. *Proc. Natl. Acad. Sci. U. S. A.* **2021**, *118* (42), No. e2110472118.

(5) Veres, P. R.; Neuman, J. A.; Bertram, T. H.; Assaf, E.; Wolfe, G. M.; Williamson, C. J.; Weinzierl, B.; Tilmes, S.; Thompson, C. R.; Thames, A. B.; et al. Global airborne sampling reveals a previously unobserved dimethyl sulfide oxidation mechanism in the marine atmosphere. *Proc. Natl. Acad. Sci. U. S. A.* **2020**, *117* (9), 4505−4510.

(6) Fung, K. M.; Heald, C. L.; Kroll, J. H.; Wang, S.; Jo, D. S.; Gettelman, A.; Lu, Z.; Liu, X.; Zaveri, R. A.; Apel, E. C. Exploring dimethyl sulfide (DMS) oxidation and implications for global aerosol radiative forcing. *Atmos. Chem. Phys.* **2022**, *22* (2), 1549−1573.

(7) Tashmim, L.; Porter, W. C.; Chen, Q.; Alexander, B.; Fite, C. H.; Holmes, C. D.; Pierce, J. R.; Croft, B.; Ishino, S. Contribution of expanded marine sulfur chemistry to the seasonal variability of dimethyl sulfide oxidation products and size-resolved sulfate aerosol. *Atmos. Chem. Phys.* **2024**, *24* (6), 3379−3403.

(8) Jacob, L. S. D.; Harvey, B. E. H.; Giorio, C.; Archibald, A. T. Determining the key sources of uncertainty in dimethyl sulfide and methanethiol oxidation under tropical, temperate, and polar marine conditions. *Atmos. Chem. Phys.* **2026**, *26* (5), 3567−3587.

(9) Jernigan, C. M.; Cappa, C. D.; Bertram, T. H. Reactive Uptake of Hydroperoxymethyl Thioformate to Sodium Chloride and Sodium Iodide Aerosol Particles. *J. Phys. Chem. A* **2022**, *126* (27), 4476−4481.

(10) Jernigan, C. M.; Fite, C. H.; Vereecken, L.; Berkelhammer, M. B.; Rollins, A. W.; Rickly, P. S.; Novelli, A.; Taraborrelli, D.; Holmes, C. D.; Bertram, T. H. Efficient Production of Carbonyl Sulfide in the Low-NOx Oxidation of Dimethyl Sulfide. *Geophys. Res. Lett.* **2022**, *49* (3), No. e2021GL096838.

(11) Jernigan, C. M.; Rivard, M. J.; Berkelhammer, M. B.; Bertram, T. H. Sulfate and Carbonyl Sulfide Production in Aqueous Reactions of Hydroperoxymethyl Thioformate. *ACS EST Air* **2024**, *1* (5), 397−404.

(12) Vermeuel, M. P.; Novak, G. A.; Jernigan, C. M.; Bertram, T. H. Diel Profile of Hydroperoxymethyl Thioformate: Evidence for Surface Deposition and Multiphase Chemistry. *Environ. Sci. Technol.* **2020**, *54* (19), 12521−12529.

Downloaded from pubs.acs.org/aeacd5/article-pdf/doi/10.1021/acsestair.6c00199/6868709/acsestair.6c00199.pdf by UNIV OF YORK user on 06 October 2026

(13) Vereecken, L.; Novelli, A.; Taraborrelli, D.; Wahner, A. Perhemiacetal formation and Cl/NO 3-initiated chemistry of hydroperoxymethylthioformate (HPMTF) in atmospheric DMS oxidation. *Environ. Sci.: Atmos.* **2025**, *5* (2), 181−190.
(14) Khan, M. A. H.; Bannan, T. J.; Holland, R.; Shallcross, D. E.; Archibald, A. T.; Matthews, E.; Back, A.; Allan, J.; Coe, H.; Artaxo, P.; Percival, C. J. Impacts of hydroperoxymethyl thioformate on the global marine sulfur budget. *ACS Earth Space Chem.* **2021**, *5* (10), 2577−2586.
(15) Holmes, C. D.; Bertram, T. H.; Confer, K. L.; Graham, K. A.; Ronan, A. C.; Wirks, C. K.; Shah, V. The role of clouds in the tropospheric NOx cycle: A new modeling approach for cloud chemistry and its global implications. *Geophys. Res. Lett.* **2019**, *46* (9), 4980−4990.
(16) Kilgour, D. B.; Jernigan, C. M.; Garmash, O.; Aggarwal, S.; Zhou, S.; Mohr, C.; Salter, M. E.; Thornton, J. A.; Wang, J.; Zieger, P.; et al. Cloud processing of dimethyl sulfide (DMS) oxidation products limits sulfur dioxide (SO2) and carbonyl sulfide (OCS) production in the eastern North Atlantic marine boundary layer. *Atmos. Chem. Phys.* **2025**, *25* (3), 1931−1947.
(17) Chace, W. S.; Womack, C.; Ball, K.; Bates, K. H.; Bohn, B.; Coggon, M.; Crounse, J. D.; Fuchs, H.; Gilman, J.; Gkatzelis, G. I.; et al. Ozone Production Efficiencies in the Three Largest United States Cities from Airborne Measurements. *Environ. Sci. Technol.* **2025**, *59* (26), 13306−13318.
(18) Robinson, M. A.; Neuman, J. A.; Huey, L. G.; Roberts, J. M.; Brown, S. S.; Veres, P. R. Temperature-dependent sensitivity of iodide chemical ionization mass spectrometers. *Atmos. Meas. Tech.* **2022**, *15* (14), 4295−4305.
(19) Lee, B. H.; Lopez-Hilfiker, F. D.; Mohr, C.; Kurtén, T.; Worsnop, D. R.; Thornton, J. A. An iodide-adduct high-resolution time-of-flight chemical-ionization mass spectrometer: Application to atmospheric inorganic and organic compounds. *Environ. Sci. Technol.* **2014**, *48* (11), 6309−6317.
(20) Veres, P.; Gilman, J.; Roberts, J.; Kuster, W.; Warneke, C.; Burling, I.; De Gouw, J. Development and validation of a portable gas phase standard generation and calibration system for volatile organic compounds. *Atmos. Meas. Tech. Discuss.* **2010**, *3* (1), 333−357.
(21) (a) Coggon, M. M.; Stockwell, C. E.; Claflin, M. S.; Pfannerstill, E. Y.; Xu, L.; Gilman, J. B.; Marcantonio, J.; Cao, C.; Bates, K.; Gkatzelis, G. I.; et al. Identifying and correcting interferences to PTR-ToF-MS measurements of isoprene and other urban volatile organic compounds. *Atmos. Meas. Tech.* **2024**, *17* (2), 801−825. (b) Yuan, B.; Koss, A. R.; Warneke, C.; Coggon, M.; Sekimoto, K.; de Gouw, J. A. Proton-transfer-reaction mass spectrometry: applications in atmospheric sciences. *Chem. Rev.* **2017**, *117* (21), 13187−13229. (c) Krechmer, J.; Lopez-Hilfiker, F.; Koss, A.; Hutterli, M.; Stoermer, C.; Deming, B.; Kimmel, J.; Warneke, C.; Holzinger, R.; Jayne, J.; et al. Evaluation of a New Reagent-Ion Source and Focusing Ion−Molecule Reactor for Use in Proton-Transfer-Reaction Mass Spectrometry. *Anal. Chem.* **2018**, *90* (20), 12011−12018.
(22) (a) Xu, L.; Coggon, M. M.; Stockwell, C. E.; Gilman, J. B.; Robinson, M. A.; Breitenlechner, M.; Lamplugh, A.; Neuman, J. A.; Novak, G. A.; Veres, P. R. A chemical ionization mass spectrometry utilizing ammonium ions (nh 4+ cims) for measurements of organic compounds in the atmosphere. *Atmos. Meas. Tech. Discuss.* **2022**, *15*, 7353−7373. (b) Zaytsev, A.; Breitenlechner, M.; Koss, A. R.; Lim, C. Y.; Rowe, J. C.; Kroll, J. H.; Keutsch, F. N. Using collision-induced dissociation to constrain sensitivity of ammonia chemical ionization mass spectrometry (NH4+ CIMS) to oxygenated volatile organic compounds. *Atmos. Meas. Technol.* **2019**, *12* (3), 1861−1870. (c) Goss, M. B.; Kroll, J. H. Chamber studies of OH+ dimethyl sulfoxide and dimethyl disulfide: insights into the dimethyl sulfide oxidation mechanism. *Atmos. Chem. Phys.* **2024**, *24* (2), 1299−1314.
(23) Barnes, I.; Hjorth, J.; Mihalopoulos, N. Dimethyl sulfide and dimethyl sulfoxide and their oxidation in the atmosphere. *Chem. Rev.* **2006**, *106* (3), 940−975.
(24) Assaf, E.; Finewax, Z.; Marshall, P.; Veres, P. R.; Neuman, J. A.; Burkholder, J. B. Measurement of the intramolecular hydrogen-shift rate coefficient for the CH3SCH2OO radical between 314 and 433 K. *J. Phys. Chem. A* **2023**, *127* (10), 2336−2350.
(25) (a) Enami, S.; Nakano, Y.; Hashimoto, S.; Kawasaki, M.; Aloisio, S.; Francisco, J. S. Reactions of Cl atoms with dimethyl sulfide: A theoretical calculation and an experimental study with cavity ring-down spectroscopy. *J. Phys. Chem. A* **2004**, *108* (39), 7785−7789. (b) Stickel, R.; Nicovich, J.; Wang, S.; Zhao, Z.; Wine, P. Kinetic and mechanistic study of the reaction of atomic chlorine with dimethyl sulfide. *J. Phys. Chem.* **1992**, *96* (24), 9875−9883.
(26) (a) Wu, R.; Wang, S.; Wang, L. New mechanism for the atmospheric oxidation of dimethyl sulfide. The importance of intramolecular hydrogen shift in a CH3SCH2OO radical. *J. Phys. Chem. A* **2015**, *119* (1), 112−117. (b) Finewax, Z.; Assaf, E.; Rollins, A. W.; Burkholder, J. B. Rate Coefficient Measurements for the CH3SCH2OO Radical + NO Reaction Between 313 and 413 K. *Int. J. Chem. Kinet.* **2025**, *57* (6), 391−399.
(27) (a) Brock, C. A.; Schröder, F.; Kärcher, B.; Petzold, A.; Busen, R.; Fiebig, M. Ultrafine particle size distributions measured in aircraft exhaust plumes. *J. Geophys. Res.: Atmos.* **2000**, *105* (D21), 26555−26567. (b) Williamson, C.; Kupc, A.; Wilson, J.; Gesler, D. W.; Reeves, J. M.; Erdesz, F.; McLaughlin, R.; Brock, C. A. Fast time response measurements of particle size distributions in the 3−60 nm size range with the nucleation mode aerosol size spectrometer. *Atmos. Meas. Technol.* **2018**, *11* (6), 3491−3509.
(28) Kupc, A.; Williamson, C.; Wagner, N. L.; Richardson, M.; Brock, C. A. Modification, calibration, and performance of the Ultra-High Sensitivity Aerosol Spectrometer for particle size distribution and volatility measurements during the Atmospheric Tomography Mission (ATom) airborne campaign. *Atmos. Meas. Tech.* **2018**, *11* (1), 369−383.
(29) Brock, C. A.; Williamson, C.; Kupc, A.; Froyd, K. D.; Erdesz, F.; Wagner, N.; Richardson, M.; Schwarz, J. P.; Gao, R.-S.; Katich, J. M.; Campuzano-Jost, P. Aerosol size distributions during the Atmospheric Tomography Mission (ATom): Methods, uncertainties, and data products. *Atmos. Meas. Tech.* **2019**, *12* (6), 3081−3099.
(30) Laskina, O.; Morris, H. S.; Grandquist, J. R.; Qin, Z.; Stone, E. A.; Tivanski, A. V.; Grassian, V. H. Size Matters in the Water Uptake and Hygroscopic Growth of Atmospherically Relevant Multicomponent Aerosol Particles. *J. Phys. Chem. A* **2015**, *119* (19), 4489−4497.
(31) Dollner, M. *Assessment of the global distribution of coarse-mode aerosol and clouds with large-scale in situ aircraft observations*; IEA, 2022.
(32) Smith, S.; Lee, J.; Bloss, W.; Johnson, G.; Ingham, T.; Heard, D. Concentrations of OH and HO 2 radicals during NAMBLEX: measurements and steady state analysis. *Atmos. Chem. Phys.* **2006**, *6* (5), 1435−1453.
(33) Levine, S.; Schwartz, S. In-cloud and below-cloud scavenging of nitric acid vapor. *Atmos. Environ.* **1982**, *16* (7), 1725−1734.
(34) (a) Partington, J. R. *An Advanced Treatise on Physical Chemistry: The Properties of Liquids*; Longmans Green, 1949. (b) Tang, M. J.; Shiraiwa, M.; Pöschl, U.; Cox, R. A.; Kalberer, M. Compilation and evaluation of gas phase diffusion coefficients of reactive trace gases in the atmosphere: Volume 2. Diffusivities of organic compounds, pressure-normalised mean free paths, and average Knudsen numbers for gas uptake calculations. *Atmos. Chem. Phys.* **2015**, *15* (10), 5585−5598.
(35) Johnson, M. T. A numerical scheme to calculate temperature and salinity dependent air-water transfer velocities for any gas. *Ocean Sci.* **2010**, *6* (4), 913−932.
(36) Bohn, B.; Lohse, I. Optical receiver characterizations and corrections for ground-based and airborne measurements of spectral actinic flux densities. *Atmos. Meas. Tech.* **2023**, *16* (2), 209−233.
(37) Hannun, R. A.; Swanson, A. K.; Bailey, S. A.; Hanisco, T. F.; Bui, T. P.; Bourgeois, I.; Peischl, J.; Ryerson, T. B. A cavity-enhanced ultraviolet absorption instrument for high-precision, fast-time-response ozone measurements. *Atmos. Meas. Tech.* **2020**, *13* (12), 6877−6887.

Downloaded from pubs.acs.org/aeacd5/article-pdf/doi/10.1021/acsestair.6c00199/6868370/acsestair.6c00199.pdf by UNIV OF YORK user on 06 October 2026

https://doi.org/10.1021/acsestair.6c00199
ACS EST Air XXXX, XXX, XXX−XXX

(38) Rollins, A. W.; Rickly, P. S.; Gao, R.-S.; Ryerson, T. B.; Brown, S. S.; Peischl, J.; Bourgeois, I. Single-photon laser-induced fluorescence detection of nitric oxide at sub-parts-per-trillion mixing ratios. *Atmos. Meas. Tech.* **2020**, *13* (5), 2425−2439.
(39) Fuchs, H.; Stainsby, A.; Berg, F.; Dubus, R.; Färber, M.; Hofzumahaus, A.; Holland, F.; Bates, K. H.; Brown, S. S.; Coggon, M. M.; et al. Advances in an OH reactivity instrument for airborne field measurements. *Atmos. Meas. Technol.* **2025**, *18* (4), 881−895.
(40) Gelaro, R.; McCarty, W.; Suárez, M. J.; Todling, R.; Molod, A.; Takacs, L.; Randles, C. A.; Darmenov, A.; Bosilovich, M. G.; Reichle, R.; Wargan, K. The modern-era retrospective analysis for research and applications, version 2 (MERRA-2). *J. Clim.* **2017**, *30* (14), 5419−5454.
(41) Miles, N. L.; Verlinde, J.; Clothiaux, E. E. Cloud droplet size distributions in low-level stratiform clouds. *J. Atmos. Sci.* **2000**, *57* (2), 295−311.
(42) Hanson, D. R.; Ravishankara, A.; Solomon, S. Heterogeneous reactions in sulfuric acid aerosols: A framework for model calculations. *J. Geophys. Res.: Atmos.* **1994**, *99* (D2), 3615−3629.
(43) Wilke, C. R.; Chang, P. Correlation of diffusion coefficients in dilute solutions. *AIChE J.* **1955**, *1* (2), 264−270.
(44) Seinfeld, J. H.; Pandis, S. N. *Atmospheric chemistry and physics: From air pollution to climate change*; John Wiley & Sons, 2016.
(45) De Bruyn, W.; Shorter, J. A.; Davidovits, P.; Worsnop, D.; Zahniser, M.; Kolb, C. Uptake of gas phase sulfur species methanesulfonic acid, dimethylsulfoxide, and dimethyl sulfone by aqueous surfaces. *J. Geophys. Res.: Atmos.* **1994**, *99* (D8), 16927−16932.
(46) Magi, L.; Schweitzer, F.; Pallares, C.; Cherif, S.; Mirabel, P.; George, C. Investigation of the uptake rate of ozone and methyl hydroperoxide by water surfaces. *J. Phys. Chem. A* **1997**, *101* (27), 4943−4949.
(47) Hanson, D. Mass Accommodation of H2SO4 and CH3SO3H on Water− Sulfuric Acid Solutions from 6% to 97% RH. *J. Phys. Chem. A* **2005**, *109* (31), 6919−6927.
(48) USEPA *Estimation Programs Interface Suite for Microsoft® Windows, v 4.11.*; United States Environmental Protection Agency: Washington, DC, USA, 2025.
(49) Meylan, W. M.; Howard, P. H. Bond contribution method for estimating Henry's law constants. *Environ. Toxicol. Chem.* **1991**, *10* (10), 1283−1293.
(50) (a) Ebert, R.-U.; Kühne, R.; Schüürmann, G. Octanol/Air Partition Coefficient− A General-Purpose Fragment Model to Predict Log K oa from Molecular Structure. *Environ. Sci. Technol.* **2023**, *57* (2), 976−984. (b) Raventos-Duran, T.; Camredon, M.; Valorso, R.; Mouchel-Vallon, C.; Aumont, B. Structure-activity relationships to estimate the effective Henry's law constants of organics of atmospheric interest. *Atmos. Chem. Phys.* **2010**, *10* (16), 7643−7654.
(51) (a) Rios, J. C. R. *Atmospheric chemistry of isoprene hydroxyhydroperoxides*; Harvard University, 2018. (b) Watts, S. F.; Brimblecombe, P. The Henry's law constant of dimethyl sulphoxide. *Environ. Technol. Lett.* **1987**, *8* (1−12), 483−486.
(52) Thamm, J.; Wolff, S.; Turner, W.; Gäb, S.; Thomas, W.; Zabel, F.; Fink, E.; Becker, K. Proof of the formation of hydroperoxymethyl formate in the ozonolysis of ethene: synthesis and FT-IR spectra of the authentic compound. *Chem. Phys. Lett.* **1996**, *258* (1−2), 155−158.
(53) (a) Adewuyi, Y. G.; Carmichael, G. R. Kinetics of oxidation of dimethyl sulfide by hydrogen peroxide in acidic and alkaline medium. *Environ. Sci. Technol.* **1986**, *20* (10), 1017−1022. (b) Chu, J.-W.; Trout, B. L. On the mechanisms of oxidati on of organic sulfides by H2O2 in aqueous solutions. *J. Am. Chem. Soc.* **2004**, *126* (3), 900−908. (c) Gershenzon, M.; Davidovits, P.; Jayne, J.; Kolb, C.; Worsnop, D. Simultaneous uptake of DMS and ozone on water. *J. Phys. Chem. A* **2001**, *105* (29), 7031−7036.
(54) Pagonis, D.; Ziemann, P. J. Chemistry of hydroperoxycarbonyls in secondary organic aerosol. *Aerosol. Sci. Technol.* **2018**, *52* (10), 1178−1193.
(55) Barnard, D. Oxidation of organic sulphides. Part IX. The reaction of ozone with organic sulphur compounds. *J. Chem. Soc.* **1957**, *160*, 4547−4555.

Downloaded from pubs.acs.org/aeacd5/article-pdf/doi/10.1021/acsestair.6c00199/6868370/acsestair.6c00199.pdf by UNIV OF YORK user on 06 October 2026

https://doi.org/10.1021/acsestair.6c00199
ACS EST Air XXXX, XXX, XXX−XXX